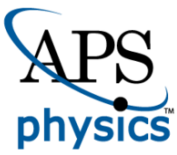

Strong Coupling Phases of Partially Filled Twisted Bilayer Graphene Narrow Bands

Jian Kang and Oskar Vafek

Phys. Rev. Lett. **122**, 246401 — Published 18 June 2019

DOI: 10.1103/PhysRevLett.122.246401

Strong coupling phases of partially filled twisted bilayer graphene narrow bands

Jian Kang[1,*] and Oskar Vafek[1,2,†]

[1] *National High Magnetic Field Laboratory, Tallahassee, Florida, 32304, USA*
[2] *Department of Physics, Florida State University, Tallahassee, Florida 32306, USA*

We identify states favored by Coulomb interactions projected onto the Wannier basis of the four narrow bands of the "magic angle" twisted bilayer graphene. At the filling of two electrons/holes per moire unit cell, such interactions favor an insulating $SU(4)$ ferromagnet. The kinetic terms select the ground state in which the two valleys with opposite spins are equally mixed, with vanishing magnetic moment per particle. We also find extended excited states, the gap to which decreases in magnetic field. An insulating stripe ferromagnetic phase is favored at one electron/hole per unit cell.

In addition to superconductivity, recent experiments on magic angle twisted bilayer graphene revealed insulating phases at carrier concentrations corresponding to partial occupation of the four narrow bands composite near the neutrality point [1–3]. Such correlated insulator phases seem to occur only when the bandwidth of the composite is reduced either by fine-tuning of the twist angle to the vicinity of the "magic" value $\sim 1.1^\circ$ or by tuning the applied pressure at $\sim 1.3^\circ$ [1–3]. Importantly, the insulating states occur at *commensurate* (rational) fillings corresponding to 2 electrons/holes per moire unit cell, with additional resistance peaks observed at fillings of 1 hole/electron per unit cell and 3 holes/electrons per unit cell [1–3]. This observation is hard to reconcile with the notion that the insulation is due to Fermi surface nesting, or the van Hove singularities, reconstructed by electron-electron interactions, because such band structure features generically occur at *incommensurate* fillings. Instead, the above observations suggest that the effective Coulomb interaction dominates the effective kinetic energy[1, 3]. The former is given by the projection of the Coulomb interaction onto the Hilbert space spanned by the narrow bands and is $\sim e^2/\epsilon\ell_m \sim 25meV$, where the moire period $\ell_m \sim 13nm$. The effective dielectric constant of the encapsulating boron nitride is estimated as $\epsilon = \sqrt{\epsilon_\perp \epsilon_\parallel} \approx 4.4$, where $\epsilon_\parallel = 6.6$ and $\epsilon_\perp = 3.0$ [4]. The kinetic energy scale is given by the bandwidth. Although there is no direct measurement of the bandwidth, theoretical calculations routinely find it to be $\lesssim 10$meV [1, 5–10]. Finally, the superlattice band gap which separates the narrow bands from the rest of the bands is extracted from transport activation gaps to be $\sim 30 - 40$meV [1, 3].

Such considerations hint that, even if the physical system is ultimately in an intermediate coupling regime, a strong coupling approach may be more successful in capturing the nature of the correlated phases. In this approach the interaction-only Hamiltonian is minimized first, and the kinetic energy term is then treated as a perturbation[8, 11–20].

Here we present the analysis and the solution to the strong coupling limit by projecting the Coulomb interaction onto the microscopically constructed exponentially localized Wannier states (WSs) for the four narrow bands [7]. In doing so we find that there is a qualitative difference between the effect of the interactions in twisted bilayer graphene narrow bands and the much studied narrow band whose width is small due to the exponentially vanishing overlap of the well separated localized orbitals i.e. a solid in an atomic limit. In contrast, the small bandwidth in twisted bilayer graphene is a result of fine tuning (twist angle or pressure) and subtle interference of the WSs, and, unlike in the atomic limit, it is not necessarily a result of large spatial separation of the exponentially localized WSs. Indeed, as shown before, each WS of the twisted bilayer graphene narrow bands has three main peaks on neighboring sites of the triangular moire superlattice [6–8]. Therefore, for nearest neighbor WSs on say, sites i and j, two peaks overlap significantly (see Fig.1). Even though the integral under both has to vanish by orthogonality, the integral under each separately does not. This leads to a dramatically new form of the interaction Hamiltonian projected onto the narrow band basis – containing terms beyond the "cluster Hubbard" term [8, 12] – which in turn leads to different strong coupling phases as in the atomic limit. Specifically, the usual anti-ferromagnetic super-exchange mechanism fails and turns ferromagnetic. Due to approximate spin-valley $SU(4)$ symmetry, the fully spin-valley polarized ferromagnet is found to be degenerate with a spin-valley entangled state whose average total magnetic moment per particle vanishes. We also find exact excited states, which are spatially extended, and whose gap is suppressed by Zeeman coupling to an external magnetic field, making it (or at least its order parameter) a candidate for the experimentally observed correlated insulator at 2 electrons/holes per moire unit cell. At 1 particle per moire unit cell we find that the projected interactions favor an insulating stripe $SU(4)$ ferromagnet. This state may be a candidate for the insulator observed at the 1/8 filling [3] if the $SU(4)$ degeneracy is lifted in favor of the physical spin ferromagnet.

We start by writing the full Hamiltonian as

$$H = K + U, \tag{1}$$

where the kinetic energy K is described by the tight-

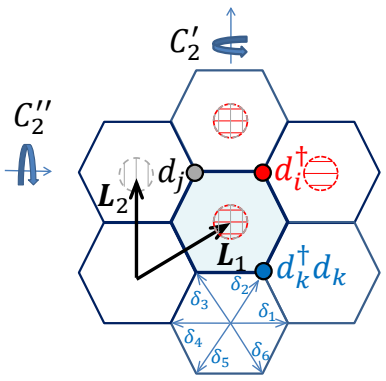

Figure 1. The centers of the hexagons correspond to the triangular moire lattice spanned by primitive vectors $\mathbf{L}_{1,2}$. The Wannier state (WS) wavefunction centered on the moire honeycomb site j has three peaks at the neighboring triangular moire sites (grey circles with vertical stripes). The WS on the neighboring site i overlaps with it on the two hexagons (red horizontal stripes). An example of a four fermion interaction term, which is beyond the extended Hubbard model, appearing in the strong coupling Hamiltonian Eqs.(6,9-11), is also shown schematically.

binding model [7] based on the WSs and where the Coulomb interaction is

$$U = \frac{1}{2}\sum_{\mathbf{r},\mathbf{r}'}\sum_{\sigma,\sigma'=\uparrow,\downarrow} c^\dagger_\sigma(\mathbf{r})c_\sigma(\mathbf{r})V(\mathbf{r}-\mathbf{r}')c^\dagger_{\sigma'}(\mathbf{r}')c_{\sigma'}(\mathbf{r}') \quad (2)$$

Projecting onto the four narrow bands is equivalent to expanding $c_\sigma(\mathbf{r})$ solely in terms of the narrow bands WSs

$$c_\sigma(\mathbf{r}) = \frac{1}{3}\sum_{\mathbf{R}}\sum_{p=1}^{6}\sum_{j=\pm1} w_{\mathbf{R}+\delta_p,j}(\mathbf{r})d_{j,\sigma}(\mathbf{R}+\delta_p)\ , \quad (3)$$

where integers m, n define the triangular moire lattice vectors $\mathbf{R} = m\mathbf{L}_1 + n\mathbf{L}_2$, the eigenvalue of the AA site centered 3-fold rotation $\exp(j2\pi i/3)$ is labeled by $j = \pm1$ and $\delta_{1,\ldots,6}$ are basis vectors connecting the honeycomb sites to the triangular sites (see Fig.1). To an excellent approximation, WSs with $j = \pm1$ correspond to different valleys with very little valley mixing[7]. The factor of $1/3$ is due to each honeycomb site position $\mathbf{R}+\boldsymbol{\delta}_p$ being counted three times.

The Coulomb interaction $V(\mathbf{r})$ is screened due to the presence of the metallic gates[1–3]. The separation between the gates sets the length-scale beyond which the image charges exponentially diminish the repulsion[21]. Interestingly, the gate separation is comparable to the moire unit cell. This, as well as the form of $w_{\mathbf{R}+\boldsymbol{\delta}_p,j}(\mathbf{r})$ justifies keeping only $\mathbf{R} = \mathbf{R}'$ in the sum below:

$$U = \frac{1}{2}\sum_{\mathbf{R},\mathbf{R}'}\sum_{\mathbf{r},\mathbf{r}'\in\hexagon}\sum_{\sigma,\sigma'=\uparrow,\downarrow} n_\sigma(\mathbf{R}+\mathbf{r})V(\mathbf{R}+\mathbf{r}-\mathbf{R}'-\mathbf{r}')n_{\sigma'}(\mathbf{R}'+\mathbf{r}') \quad (4)$$

$$\approx \frac{1}{2}\sum_{\mathbf{R}}\sum_{\mathbf{r},\mathbf{r}'\in\hexagon}\sum_{\sigma,\sigma'=\uparrow,\downarrow} n_\sigma(\mathbf{R}+\mathbf{r})V(\mathbf{r}-\mathbf{r}')n_{\sigma'}(\mathbf{R}'+\mathbf{r}'), \quad (5)$$

where $n_\sigma(\mathbf{r}) = c^\dagger_\sigma(\mathbf{r})c_\sigma(\mathbf{r})$ and the sums over $\mathbf{r},\mathbf{r}'$ are restricted to be within the moire hexagon centered at the origin (see shaded $\hexagon$ in Fig.1).

Substituting the Eq.(3) into the above form, with numerically calculated $w_{\mathbf{R}+\delta_p,j}(\mathbf{r})$ from the microscopic model [7] we find that to an excellent approximation we can replace $V(\mathbf{r}-\mathbf{r}')$ by its average over a region of size set by the extent of $w_{\delta_p,j}(\mathbf{r})$ within the moire hexagon V_0, and because $V(\mathbf{r})$ is dominated by the small wavevectors, we can ignore the valley mixing terms [6]. Thus,

$$U \approx \frac{V_0}{2}\sum_{\mathbf{R}}\left(\sum_{j=\pm1}\sum_{\sigma=\uparrow,\downarrow} O_{j,\sigma}(\mathbf{R})\right)^2, \quad (6)$$

where $O_{j,\sigma}(\mathbf{R}) = \sum_{\mathbf{r}\in\hexagon} n_{j,\sigma}(\mathbf{R}+\mathbf{r})$ and

$$n_{j,\sigma}(\mathbf{R}+\mathbf{r}) = \frac{1}{9}\sum_{\bar{\mathbf{R}},\bar{\mathbf{R}}'}\sum_{p,p'=1}^{6} w^*_{\bar{\mathbf{R}}-\mathbf{R}+\delta_p,j}(\mathbf{r})w_{\bar{\mathbf{R}}'-\mathbf{R}+\delta_{p'},j}(\mathbf{r})d^\dagger_{j,\sigma}(\bar{\mathbf{R}}+\delta_p)d_{j,\sigma}(\bar{\mathbf{R}}'+\delta_{p'}) \quad (7)$$

$$\approx \sum_{p,p'=1}^{6} w^*_{\delta_p,j}(\mathbf{r})w_{\delta_{p'},j}(\mathbf{r})d^\dagger_{j,\sigma}(\mathbf{R}+\delta_p)d_{j,\sigma}(\mathbf{R}+\delta_{p'})\ . \quad (8)$$

It is clear that $O_{j,\sigma}(\mathbf{R})$ is a superposition of not only density-like operators $d^\dagger_{j,\sigma}(\mathbf{R}+\delta_p)d_{j,\sigma}(\mathbf{R}+\delta_{p'})$ with

$p = p'$, but also hopping-like terms with $p \neq p'$ which may be of the same order of magnitude. For example, $\sum_{\mathbf{r}\in\hexagon} w^*_{\delta_p,j}(\mathbf{r}) w_{\delta_{p+1},j}(\mathbf{r})$ is non-negligible. This is despite the WSs being orthogonal when $\mathbf{r}$ is summed over *all* space; with $\mathbf{r}$ restricted to only one hexagon, the sum is $\mathcal{O}(1)$. For fixed $\mathbf{R}$, the orthogonality in turn forces terms such as those with $p = 1$ and $p' = 2$ to be negative of the terms with $p = 5$ and $p' = 4$, etc. In what follows, we assume for clarity that the 3 peaks of each WS reside entirely within the 3 neighboring hexagons with no support elsewhere. We relax this assumption in the Supplementary material without any change to our conclusions [22]. To summarize,

$$O_{j,\sigma}(\boldsymbol{R}) = \frac{1}{3} Q_{j,\sigma}(\boldsymbol{R}) + \alpha_1 T_{j,\sigma}(\boldsymbol{R}) \ , \quad \text{where} \tag{9}$$

$$Q_{j,\sigma}(\boldsymbol{R}) = \sum_{p=1}^{6} d^\dagger_{j,\sigma}(\boldsymbol{R}+\boldsymbol{\delta}_p) d_{j,\sigma}(\boldsymbol{R}+\boldsymbol{\delta}_p), \tag{10}$$

$$T_{j,\sigma}(\boldsymbol{R}) = \sum_{p=1}^{6} \left(e^{i\eta_{p,j}} d^\dagger_{j,\sigma}(\boldsymbol{R}+\boldsymbol{\delta}_{p+1}) d_{j,\sigma}(\boldsymbol{R}+\boldsymbol{\delta}_p) + h.c. \right), \tag{11}$$

where $e^{i\eta_{p,j}} = (-)^{p-1} e^{i(-)^{p-1}\theta_j}$, $\boldsymbol{\delta}_7 = \boldsymbol{\delta}_1$, and

$$\alpha_1 e^{i\theta_j} = \textstyle\sum_{\boldsymbol{r}\in\hexagon} w^*_{\boldsymbol{R}+\boldsymbol{\delta}_2,j,\sigma}(\boldsymbol{r}) w_{\boldsymbol{R}+\boldsymbol{\delta}_1,j,\sigma}(\boldsymbol{r}). \tag{12}$$

$\alpha_1 e^{i\theta_j}$ is generally a complex number and $\theta_{+1} = -\theta_{-1}$. This phase factor can be absorbed by applying a global $U(1)$ transformation on WSs. In the rest of the paper, we will therefore assume $\theta_{+1} = -\theta_{-1} = 0$. For our WSs constructed from the projection method [22], $\alpha_1 \approx 0.23$. Although not all the above interaction terms have been included in the model of Ref. [6], and although the Coulomb interaction is not assumed screened in Ref.[6], similar value for α_1 can be estimated from their ratio of the nearest-neighbor exchange and nearest neighbor density repulsion as $\alpha_1^{(K)} \approx \frac{1}{3}\sqrt{J_1/V_1} \approx 0.16$ (see Table I of Ref.[6]); see also [28]. The nature of the ground state in the strong coupling limit is insensitive to such differences.

We emphasize that it is not necessary to include the kinetic energy terms K in Eq.(1) to induce correlation among various sites; such sizable value of α_1 makes the projected interaction term (6) non-local *even in the strong coupling limit*, and as we will see it dictates the nature of the ground state. It is therefore worth understanding why α_1 is sizable. In the atomic limit, this overlap is exponentially small. As a consequence, the interactions usually include only the on-site terms, giving rise to the Hubbard model; α_1 would then be set by the ratio of the bandwidth and the on-site repulsion. In our case, as mentioned, the two of the three peaks of the neighboring WSs spatially overlap and $\alpha_1 \sim \mathcal{O}(1)$. This stems from the fact that the emergent two-fold symmetry C_2'' (see Fig.1) is not locally implemented for our valley filtered WSs [23]. Otherwise, when combined with (locally implemented) C_2' (see Fig.1) and the emergent valley $U(1)$ symmetry, all the WSs would have to have the same parity under C_2''[23], leading to $\alpha_1 = 0$. However, C_2'' cannot be locally implemented simultaneously with the valley $U(1)$, C_2', and the time reversal symmetry[8, 23]. $\alpha_1 \sim \mathcal{O}(1)$ is thus rooted in the non-trivial topological properties of the narrow bands[8, 23–27].

As the first step, we therefore need to find the spectrum of the interaction U in Eqn. (6). This is non-trivial because the commutator $[O_{\sigma,j}(\mathbf{R}), O_{\sigma,j}(\mathbf{R}')]$ does not vanish for nearest neighbors $\mathbf{R}$ and $\mathbf{R}'$ due to $\alpha_1 \neq 0$. However, the ground state of (6) can be exactly solved for special fillings, including 2 particles/holes per unit cell. To see this, note that $\sum_{\mathbf{R}} \sum_j \sum_\sigma O_{j,\sigma}(\mathbf{R}) = \hat{N}$, where $\hat{N}$ is the total particle number operator. Therefore, we can write (6) exactly as

$$\frac{V_0}{2} \sum_{\mathbf{R}} \left(n_0 - \sum_{j,\sigma} O_{j,\sigma}(\mathbf{R}) \right)^2 + V_0 n_0 \hat{N} - \frac{V_0}{2} n_0^2 N_{\mathbf{R}} \tag{13}$$

where $N_{\mathbf{R}}$ is the total number of moire unit cells. Because $\hat{N}$ is fixed in the quantum number sector of interest, the last two terms are fixed. The ground state thus minimizes the first term. But the first term is a sum of squares of Hermitian operators, and if we can find a state in which each term vanishes, we find the ground state. Let $n_0 = 2$. Then the state

$$|\Phi_0\rangle = \prod_{\mathbf{R}} d^\dagger_{j=1,\uparrow}(\mathbf{R}+\boldsymbol{\delta}_1) d^\dagger_{j=1,\uparrow}(\mathbf{R}+\boldsymbol{\delta}_2)|0\rangle \tag{14}$$

makes the first term vanish for every $\mathbf{R}$, and is therefore a ground state. This state actually corresponds to a fully spin/valley polarized ferromagnet with two electrons per moire unit cell.

This result can be recovered in the basis of Bloch states. Starting with the most general Coulomb interaction $\hat{V} = \frac{1}{2}\sum_{\boldsymbol{q}} V(\boldsymbol{q}) \rho_{\boldsymbol{q}} \rho_{-\boldsymbol{q}}$ with $V(\boldsymbol{q}) > 0$ and $\rho_q = \sum_{\sigma=\uparrow,\downarrow} \sum_{\mathbf{r}} e^{-i\mathbf{q}\cdot\mathbf{r}} n_\sigma(\mathbf{r})$, we project it to the Bloch basis of the four narrow bands. Assuming no valley mixing, the state

$$|\Phi_0'\rangle = \prod_{\boldsymbol{k}} f^\dagger_{j=1,\mu=1,\uparrow}(\boldsymbol{k}) f^\dagger_{j=1,\mu=2,\uparrow}(\boldsymbol{k})|0\rangle \ , \tag{15}$$

is the eigenstate of $\hat{V}$ with the eigenvalue of $E = \frac{1}{2}\sum_{\boldsymbol{G}} V(\boldsymbol{G}) \left|N_{j=1,\boldsymbol{G}}\right|^2$ where $\sum_{\boldsymbol{G}}$ sums over all the reciprocal lattice vectors of the moire lattice. Here $f^\dagger_{j,\mu,\sigma}$ is the creation operator for the Bloch state in the narrow bands with the valley j, band μ, and spin σ. The Fourier transform of the charge density of the state $|\Phi_0'\rangle$ is

$$N_{j\boldsymbol{G}} = \int \frac{\mathrm{d}^2 k}{(2\pi)^2} \sum_{\boldsymbol{r}\in UC} \mathrm{d}\boldsymbol{r} \ \sum_\mu |\psi_{j\mu\boldsymbol{k}}(\boldsymbol{r})|^2 \, e^{-i\boldsymbol{G}\cdot\boldsymbol{r}},$$

where the $\boldsymbol{r}$ sum is over the unit cell, and $\psi_{j\mu\boldsymbol{k}}(\boldsymbol{r})$ is the Bloch state wavefunction with the valley j, the band μ,

and the momentum $\boldsymbol{k}$. As $V(\boldsymbol{q}) > 0$, it is reasonable to expect that $|\Phi_0'\rangle$ is also the ground state if $V(\boldsymbol{q})$ decays fast enough with increasing $\boldsymbol{q}$. The states $|\Phi_0'\rangle$ and $|\Phi_0\rangle$ are equivalent, strongly suggesting that our conclusion is independent of the choice of the basis.

Although $|\Phi_0\rangle$ is a ground state, it is not the only one for the interaction in Eqn. 6. Due to the $SU(4)$ symmetry of Eq.(6), the ground state is $(2N_{\mathbf{R}}+3)(2N_{\mathbf{R}}+2)(2N_{\mathbf{R}}+1)/6$ fold degenerate. This $SU(4)$ ground state manifold includes states as (see Fig.2(a))

$$|\Phi_1\rangle = \prod_{\mathbf{R}} \prod_{p=1}^{2} \frac{1}{\sqrt{2}} \left(d^{\dagger}_{1,\uparrow}(\mathbf{R}+\delta_p) + d^{\dagger}_{-1,\downarrow}(\mathbf{R}+\delta_p) \right) |0\rangle \quad (16)$$

Note that the expectation value of the square of the total (magnetic) spin operator $\langle \Phi_1 | \mathbf{S}^2_{tot} | \Phi_1 \rangle = \mathcal{O}(N_{\mathbf{R}})$, which means that the magnetic moment per particle vanishes in the thermodynamic limit. $|\Phi_1\rangle$ is therefore not a ferromagnet.

The ground state degeneracy is lifted by the kinetic terms, K in Eq.(1), which in general break the $SU(4)$ symmetry. The valley $U(1)$ symmetric hopping terms $t(\boldsymbol{R}+\boldsymbol{\delta}, \boldsymbol{R}'+\boldsymbol{\delta}') d^{\dagger}_{\boldsymbol{R}+\boldsymbol{\delta},j,\sigma} d_{\boldsymbol{R}'+\boldsymbol{\delta}',j,\sigma}$ favor the state with two valleys equally mixed, because then the second order process is least blocked. For the same reason the hopping terms that mix the valleys favor the state in which the two valleys carry opposite spins. The ground states is then given by Eqn. 16 up to a global spin $SU(2)$ rotation. The non-magnetic ground state depicted in Fig.2(a) is thus favored by the kinetic terms.

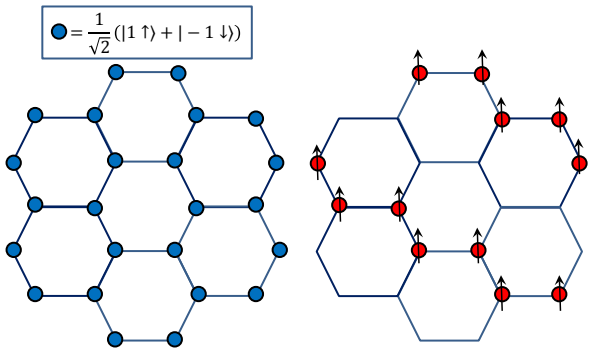

Figure 2. Schematic of the ground states at (a) 1/4 filling (2 electrons/holes per moire unit cell) and at (b) 1/8 filling (1 electron/hole per moire unit cell).

We can also find some of the excited eigenstates of Eq.(6) exactly. In particular,

$$|N+1, j, \sigma; p \mod 2\rangle = \sum_{\mathbf{R}} d^{\dagger}_{j,\sigma}(\mathbf{R}+\delta_p)|\Phi_1\rangle, \quad (17)$$

$$|N-1, j, \sigma; p \mod 2\rangle = \sum_{\mathbf{R}} d_{j,\sigma}(\mathbf{R}+\delta_p)|\Phi_1\rangle, \quad (18)$$

have energies $E_{N+1} = \frac{13}{6}V_0 + E_N$ and $E_{N-1} = -\frac{11}{6}V_0 + E_N$, respectively, where $E_N = 2N_{\mathbf{R}}V_0$. The gap is therefore at most $\Delta = E_{N+1} + E_{N-1} - 2E_N = V_0/3$. Note that the excitations (17)-(18) are spatially extended.

Even though the ground state $|\Phi_1\rangle$ does not couple linearly to the Zeeman magnetic field, $\mathbf{B}$, the excitations do, and the gap closes upon the application of a critical $\mathbf{B}$.

In order to gain some intuition for the physics behind the mathematical results discussed, imagine artificially tuning α_1 to be small. At $\alpha_1 = 0$, ground states of the "cluster Hubbard" terms include states with one particle per honeycomb site. The small hopping terms give rise to exchange interactions $\mathcal{O}(\alpha_1^2)$, via both the usual second order perturbation theory and directly via the first order terms also of $\mathcal{O}(\alpha_1^2)$. The former would normally be anti-ferromagnetic, but in this case contributions from different hexagons cancel and only the latter, ferromagnetic exchange, remains [1]. The ground state manifold of the "cluster Hubbard" Hamiltonian also includes states which do not necessarily have one particle per site, but the same argument applies [22].

Recent experiments also suggest that an insulating state appears at the filling of one hole/electron per unit cell, with the insulation enhanced by the Zeeman magnetic field [3]. We were unable to find the exact ground state at this filling analytically, even in the strong coupling limit because $\alpha_1 \neq 0$. However, the ground state can be found if α_1 is small. The leading term in U is given by the "cluster Hubbard" terms, with ground states for which each hexagon contains three fermions, and $\sum_{j,\sigma} Q_{j,\sigma}(\boldsymbol{R}) = 3$. Such ground states are highly degenerate even without counting the valley and spin degrees of freedom. The linear order and the second order of the cross term $\sum_{\boldsymbol{R}} \left(\sum_{j,\sigma} Q_{j,\sigma}(\boldsymbol{R}) \right) \left(\sum_{j',\sigma'} T_{j',\sigma'}(\boldsymbol{R}) \right)$ vanish for the same reason as discussed above. Therefore, to the order $O(\alpha_1^2)$, only the term $\sum_{\boldsymbol{R}} \left(\sum_{j,\sigma} T_{j,\sigma}(\boldsymbol{R}) \right)^2$ contributes. This contribution is minimized if *(1)* each hexagon contains exactly three occupied sites; *(2)* each occupied site is in the same state; *(3)* the number of bonds connecting an occupied site and an unoccupied site is minimized. These constraints favor the stripe $SU(4)$ ferromagnetic phase as the ground state, see Fig. 2(b), with the energy correction $\delta E = \alpha_1^2 N_R V_0/2$. This phase is also an insulator due to the existence of the charge gap.

To summarize, we analysed the Coulomb interactions (screened by the gates) projected to the exponentially localized Wannier states[7] for the four narrow bands in

[1] Recently, the ferromagnetic ground state is proposed to account for the insulator phase found in trilayer graphene, with the trivial band structure [29]. However, the ferromagnetic exchange interaction in Ref. [29] is found to be one order smaller than the on-site repulsion.

the "magic angle" twisted bilayer graphene. The projected interaction is highly non-local and is beyond extended Hubbard models. Such novel interactions result from the non-trivial topological properties of the narrow bands[8, 23], giving rise to the $SU(4)$ ferromagnetic ground states at 1/4 and 1/8 filings. At 1/4 filling, the kinetic terms break the $SU(4)$ symmetry and select the state in which two valleys with opposite spins are equally mixed (Fig. 2(a)). This state, although still $SU(4)$ ferromagnetic, is (physical) spin non-magnetic in the thermodynamic limit, with a charge gap suppressed by the magnetic field. We also argue that the stripe $SU(4)$ ferromagnetic insulator phase is the ground state at 1/8 filling (Fig. 2(b)). If the $SU(4)$ degeneracy is lifted in favor of the physical spin ferromagnet, such state could be a candidate for the experimentally observed insulator at the 1/8 filling [3]. The mechanism of such symmetry breaking remains an open problem.

Note added. Recently, after the submission of our manuscript, another theoretical work [30] was posted on arXiv, which includes a subset of the interactions described in Eqn. 6 and finds the spin ferromagnetic state at one-quarter filling.

JK was supported by the National High Magnetic Field Laboratory through NSF Grant No. DMR-1157490 and the State of Florida. O. V. was supported by NSF DMR-1506756.

* jian.kang@fsu.edu
† vafek@magnet.fsu.edu

[1] Y. Cao, V. Fatemi, A. Demir, S. Fang, S. L. Tomarken, J. Y. Luo, J. D. Sanchez-Yamagishi, K. Watanabe, T. Taniguchi, E. Kaxiras, R. C. Ashoori, and P. Jarillo-Herrero, *Unconventional superconductivity in magic-angle graphene superlattices*, Nature **556**, 43 (2018).

[2] Y. Cao, V. Fatemi, S. Fang, K. Watanabe, T. Taniguchi, E. Kaxiras, and P. Jarillo-Herrero, *Correlated insulator behaviour at half-filling in magic-angle graphene superlattices*, Nature **556**, 80 (2018).

[3] M. Yankowitz, *et al.*, *Tuning superconductivity in twisted bilayer graphene*, Science 363, 1059 (2019).

[4] B. M. Hunt, *et al.*, *Direct measurement of discrete valley and orbital quantum numbers in bilayer graphene*, Nat. Commun. **8**, 948 (2017).

[5] R. Bistritzer and A.H. MacDonald, *Moire bands in twisted double-layer graphene*, PNAS **108** 12233 (2011).

[6] M. Koshino, N.F.Q. Yuan, T. Koretsune, M. Ochi, K. Kuroki, and L. Fu, *Maximally Localized Wannier Orbitals and the Extended Hubbard Model for Twisted Bilayer Graphene*, Phys. Rev. X 8, 031087 (2018).

[7] J. Kang and O. Vafek, *Symmetry, Maximally Localized Wannier States, and a Low-Energy Model for Twisted Bilayer Graphene Narrow Bands*, Phys. Rev. X 8, 031088 (2018).

[8] H. C. Po, L. Zou, A. Vishwanath, and T. Senthil, *Origin of Mott Insulating Behavior and Superconductivity in Twisted Bilayer Graphene*, Phys. Rev. X 8, 031089 (2018).

[9] X. Lin and D. Tomanek, *Minimum model for the electronic structure of twisted bilayer graphene and related structures*, Phys. Rev. B 98, 081410(R) (2018).

[10] M. Angeli, D. Mandelli, A. Valli, A. Amaricci, M. Capone, E. Tosatti, M. Fabrizio, *Emergent D_6 symmetry in fully-relaxed magic-angle twisted bilayer graphene*, Phys. Rev. B 98, 235137 (2018).

[11] C. Xu and L. Balents, *Topological Superconductivity in Twisted Multilayer Graphene*, Phys. Rev. Lett. **121**, 087001 (2018).

[12] X. Y. Xu, K. T. Law, and P. A. Lee, *Kekulé valence bond order in an extended Hubbard model on the honeycomb lattice, with possible applications to twisted bilayer graphene*, Phys. Rev. B **98**, 121406 (2018).

[13] B. Padhi, C. Setty, and P. W. Phillips, *Doped Twisted Bilayer Graphene near Magic Angles: Proximity to Wigner Crystallization not Mott Insulation*, Nano Lett. **18**, 6175 (2018).

[14] J. F. Dodaro, S. A. Kivelson, Y. Schattner, X.-Q. Sun, and C. Wang, *Phases of a phenomenological model of twisted bilayer graphene*, Phys. Rev. B **98**, 075154 (2018).

[15] A. Thomson, S. Chatterjee, S. Sachdev, M. S. Scheurer, *Triangular antiferromagnetism on the honeycomb lattice of twisted bilayer graphen*, Phys. Rev. B **98**, 075109 (2018).

[16] D. M. Kennes, J. Lischner, C. Karrasch, *Strong Correlations and d+id Superconductivity in Twisted Bilayer Graphene*, Phys. Rev. B 98, 241407 (2018).

[17] C.-M. Jian, C. Xu, *Moire Insulators viewed as the Surface of three dimensional Symmetry Protected Topological Phases*, arXiv:1810.03610.

[18] B. Padhi and P. Phillips, *Pressure-Induced Metal-Insulator Transition in Twisted Bi-layer Graphene*, arXiv:1810.00884.

[19] M. Ochi, M. Koshino, K. Kuroki, *Possible correlated insulating states in magic-angle twisted bilayer graphene under strongly competing interactions*, Phys. Rev. B **98**, 081102 (2018).

[20] J. W. F. Venderbos, R. M. Fernandes, *Correlations and electronic order in a two-orbital honeycomb lattice model for twisted bilayer graphene*, Phys. Rev. B 98, 245103 (2018).

[21] R. E. Throckmorton and O. Vafek, *Fermions on bilayer graphene: Symmetry breaking for $B = 0$ and $\nu = 0$*, Phys. Rev. B **86**, 115447 (2015).

[22] See Supplementary Material for more detailed calculations of the interaction constants and the derivation of the ground states as well as the extended excited states, which includes Ref. [1–3, 7, 21, 31, 32].

[23] L. Zou, H. C. Po, A. Vishwanath, T. Senthil, *Band Structure of Twisted Bilayer Graphene: Emergent Symmetries, Commensurate Approximants and Wannier Obstructions*, Phys. Rev. B **98**, 085435 (2018).

[24] Zhida Song, Zhijun Wang, Wujun Shi, Gang Li, Chen Fang, B. Andrei Bernevig, *All "Magic Angles" Are "Stable" Topological*, arXiv:1807.10676.

[25] H. C. Po, L. Zou, T. Senthil, A. Vishwanath, *Faithful Tight-binding Models and Fragile Topology of Magic-angle Bilayer Graphene*, arXiv:1808.02482.

[26] J. Ahn, S. Park, B.-J. Yang, *Failure of Nielsen-Ninomiya theorem and fragile topology in two-dimensional systems with space-time inversion symmetry: application to twisted bilayer graphene at magic angle*, Phys. Rev. X 9,

021013 (2019).

[27] J. Liu, J. Liu, and X. Dai, *The pseudo-Landau-level representation of twisted bilayer graphene: band topology and the implications on the correlated insulating phase*, Phys. Rev. B 99, 155415 (2019).

[28] Based on an attempt to match the Hartree-Fock theory in momentum space and a (renormalized) dispersion obtained from a tight-binding calculation, a very different form of the assisted next-nearest neighbor hopping interaction has been proposed in F. Guinea and N. R. Walet, *Electrostatic effects and band distortions in twisted graphene bilayers*, PNAS 115, 13174 (2018).

[29] Y.-H. Zhang and T. Senthil, *Bridging Hubbard Model Physics and Quantum Hall Physics in Trilayer Graphene/h-BN moiré superlattice*, arXiv:1809.05110.

[30] K. Seo, V. N. Kotov, and B. Uchoa, *Ferromagnetic Mott State in Twisted Graphene Bilayers at the Magic Angle*, arXiv:1812.02550.

[31] N. Marzari and D. Vanderbilt, *Maximally Localized Generalized Wannier Functions for Composite Energy Bands*, Phys. Rev. B **56**, 12847 (1997); N. Marzari, A. A. Mostofi, J. R. Yates, I. Souza, and D. Vanderbilt, *Maximally Localized Wannier Functions: Theory and Applications*, Rev. Mod. Phys. **84**, 1419 (2012); R. Sakuma, *Symmetry-Adapted Wannier Functions in the Maximal Localization Procedure*, Phys. Rev. B **87**, 235109 (2013).

[32] T. O. Wehling, E. Şaşioğlu, C. Friedrich, A. I. Lichtenstein, M. I. Katsnelson, and S. Blügel, *Strength of Effective Coulomb Interactions in Graphene and Graphite*, Phys. Rev. Lett. **106**, 236805 (2011).